Vortical and acoustical mode coupling inside a porous tube with uniform wall suction

T. A. Jankowski[a] and J. Majdalani[b]
University of Tennessee Space Institute, Tullahoma, Tennessee 37388

(Received 30 January 2002; revised 18 February 2005; accepted 22 March 2005)

This paper considers the oscillatory motion of gases inside a long porous tube of the closed-open type. In particular, the focus is placed on describing an analytical solution for the internal acoustico-vortical coupling that arises in the presence of appreciable wall suction. This unsteady field is driven by longitudinal oscillatory waves that are triggered by small unavoidable fluctuations in the wall suction speed. Under the assumption of small amplitude oscillations, the time-dependent governing equations are linearized through a regular perturbation of the dependent variables. Further application of the Helmholtz vector decomposition theorem enables us to discriminate between acoustical and vortical equations. After solving the wave equation for the acoustical contribution, the boundary-driven vortical field is considered. The method of matched-asymptotic expansions is then used to obtain a closed-form solution for the unsteady momentum equation developing from flow decomposition. An exact series expansion is also derived and shown to coincide with the numerical solution for the problem. The numerically verified end results suggest that the asymptotic scheme is capable of providing a sufficiently accurate solution. This is due to the error associated with the matched-asymptotic expansion being smaller than the error introduced in the Navier-Stokes linearization. A basis for comparison is established by examining the evolution of the oscillatory field in both space and time. The corresponding boundary-layer behavior is also characterized over a range of oscillation frequencies and wall suction velocities. In general, the current solution is found to exhibit features that are consistent with the laminar theory of periodic flows. By comparison to the Sexl profile in nonporous tubes, the critically damped solution obtained here exhibits a slightly smaller overshoot and depth of penetration. These features may be attributed to the suction effect that tends to attract the shear layers closer the wall. [DOI: 10.1121/1.1905639]

PACS numbers: 43.20.Mv, 43.28.Py [LLT] Pages: 3448–3458

I. INTRODUCTION

In a previous article,[1] an asymptotic solution was presented for the acoustico-vortical field that was triggered by small fluctuations in wall injection inside a porous enclosure. This effort was supplemented by a higher-order analytical approximation based on a Liouville-Green transformation.[2] The current article extends the former studies by considering the suction-driven flow analog. In particular, the focus is presently shifted to the acoustico-vortical field inside a porous tube with appreciable wall suction. Despite the apparent resemblance with the injection-driven problem, the presence of wall suction leads to a dissimilar physical setting requiring a separate mathematical treatment. The new treatment applies to the linearized Navier-Stokes equations obtained through flow decomposition.

Suction-induced flows that are susceptible to acoustical oscillations are encountered in diverse applications. One pertains to membrane filtration[3,4] and the separation of uranium isotopes by differential gas diffusion.[5–7] Another arises in the modeling of mechanically assisted respiration,[8] hemodialysis in artificial kidneys,[9] and mass transport in the lungs.[10,11] A third concerns boundary-layer separation and control.[12,13] While past investigations have primarily concentrated on nonoscillatory behavior, the intent of this article is to account for possible flow periodicity that can be often introduced either internally, through a self-sustaining mechanism, or externally, through an oscillating boundary.

The inception of unavoidable fluctuations in injection-driven flows has been reported in several experimental investigations.[14–16] One source of oscillatory behavior can be ascribed to random fluctuations in the wall injection rate. These are often inevitable and take place at random frequencies. Clearly, those matching the tube's natural frequency give rise to a self-sustaining acoustical field.[14–16] Theoretical investigations suggest that similar behavior can be expected in suction-driven flows.[17–20] In some applications, however, an externally induced oscillatory field can exist. This is true when the field is created from laboratory-controlled wave generators, or from periodic sources supplied by autonomous mechanisms. Examples of the latter include the peristaltic mechanisms in control of respiratory and circulatory functions.

Whether the time dependence comes through self-induced or externally triggered sources, the goal of this study is to incorporate these oscillations into the suction-driven

[a]Current address: Los Alamos National Laboratory, Engineering Sciences and Applications Division-Applied Engineering Technologies (ESA-AET), Los Alamos, NM 87545.
[b]Author to whom all correspondence should be addressed: Department of Mechanical, Aerospace and Biomedical Engineering, University of Tennessee (UTSI), Tullahoma, TN 37388. Electronic mail: maji@utsi.edu

flow. By virtue of the complexity of the resulting model, the outcome we seek is an approximate solution only. Unlike the mean flow counterpart,[21–24] the existence of an exact unsteady solution can be proven impossible in light of recent mathematical reports.[17–20] To the author's knowledge, the current effort may constitute the first attempt at formulating a time-dependent solution for the suction-driven field inside a porous tube.

It may be safely stated that Berman's landmark paper[5] has provided the original motivation for the suction-driven problems. This, Berman accomplished, by showing that the Navier-Stokes equations could be reduced to a nonlinear ordinary differential equation (ODE) of fourth order. Berman was also first in applying asymptotics to obtain a solution in the presence of small wall suction. In the process, Berman's perturbation parameter was quantified by the cross-flow Reynolds number $\mathrm{Re}\equiv V_s a/\nu_0$. This term was based on the wall suction velocity V_s, viscosity ν_0, and tube radius a. Based on Berman's equation, numerous studies ensued, some with the purpose of generating closed-form descriptions for suction-driven flows over different ranges of Re. By way of example, one may cite Yuan,[25,26] Sellars,[27] and Terrill,[28–30] who have extended Berman's small suction case to encompass higher ranges of Re. While Yuan extended Berman's solution up to $\mathrm{Re}=20$, Sellars and Terrill developed approximate solutions that coincided as $\mathrm{Re}\to\infty$ in both channels and tubes. In this work, their joint solution will be used to prescribe the mean flow character.

A number of mathematical studies have also addressed the important aspect of solution multiplicity.[17–24] In summary, a total of four solution types were detected in the suction-driven porous tube.[20] For small suction, two solutions were shown to exist for $0\leqslant \mathrm{Re}\leqslant 2.3$. While no solutions were present in the interval $2.3<\mathrm{Re}<9.1$, four outcomes were observed for $9.1\leqslant \mathrm{Re}<\infty$. Stability of the porous tube solution was also examined by Zaturska, Drazin, and Banks.[20] Their results have indicated that the Berman-type similarity solutions could only be stable to time-dependent perturbations in the ranges $0\leqslant \mathrm{Re}\leqslant 2.3$ and $9.113\leqslant \mathrm{Re}<44.709$. Outside these ranges, unstable solutions due to asymmetric perturbations were likely to exist. Nonetheless, despite the speculations made regarding the physicality of unstable solutions, no laboratory confirmation could be found in the technical literature. For this reason, the current study utilizes the leading-order solution for large Re as a model for the mean flow field in the presence of symmetric oscillations.

The physical idealization starts in Sec. II with a definition of the basic flow model. This is initiated with a description of the system geometry and physical criteria. In Sec. III, the governing equations are presented in their general dimensional form. Subsequently, equations and variables are normalized, linearized, and decomposed into steady and time-dependent sets.[1] The temporal field is further subdivided in Sec. IV using the Helmholtz vector superposition theorem. At the outset, acoustical and vortical equations are distinguished. While the pressure-driven response is dealt with immediately, the momentum equation obtained from the rotational component is simplified to a second-order ODE. In Sec. V the rotational momentum equation is examined before a solution is attempted. This is followed in Sec. VI by the presentation of a composite solution based on matched-asymptotic expansions. An exact series expansion is developed in Sec. VII. Finally, results are displayed and discussed in Sec. VIII. Everywhere, the scope is restricted to $\mathrm{Re}\geqslant 20$.

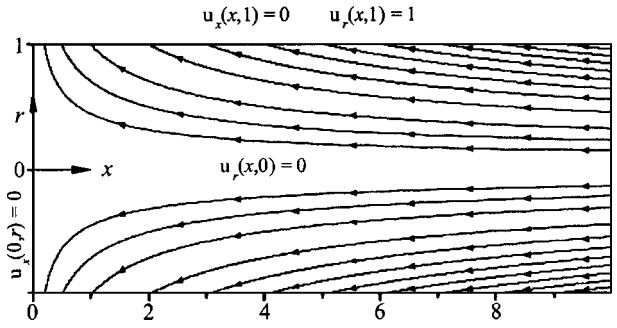

FIG. 1. Geometrical sketch showing mean flow streamlines and boundary conditions based on Terrill's large suction-flow solution.

II. THE BASIC FLOW MODEL

A. The porous tube

We shall consider a long porous tube of radius a. Fluid is extracted from the circumferential walls at a uniform wall velocity V_s. The length of the tube is defined by L and the system is simplified by imposing the condition of symmetry about the tube's axis. This choice permits the solution domain to become reducible to $0\leqslant x\leqslant l$, and $0\leqslant r\leqslant 1$, where $l=L/a$ is the dimensionless tube length. For illustrative purposes, Fig. 1 sketches a cross section of the tube with the mean flow streamlines calculated from Terrill's solution for large suction.[28]

Under the influence of small variations in the suction rate, a tube that is closed at the head end and open at the aft end can develop longitudinal pressure oscillations of amplitude A_p. The corresponding acoustical frequency can be specified by[31,32]

$$\omega_0=(m-\tfrac{1}{2})\pi a_0/L, \tag{1}$$

where a_0 is the speed of sound and m is the oscillation mode number.

B. Limiting conditions

In order to simplify the analysis to the point where an analytical solution can be arrived at, several restrictions must be observed. First, the mean flow must be Newtonian, laminar, and unsusceptible to mixing, swirling, or turbulence. Furthermore, the oscillatory pressure amplitude is taken to be small in comparison with the stagnation pressure.

III. GOVERNING EQUATIONS

A. The conservation equations

Employing asterisks to designate dimensional variables, density, pressure, time, velocity, and the shear stress tensor

can be represented by ρ^*, p^*, t^*, $\mathbf{u}^*$, and τ^*, respectively. Continuity and conservation of momentum can then be written in their general forms[33]

$$\partial\rho^*/\partial t^* + \nabla^* \cdot (\rho^* \mathbf{u}^*) = 0, \tag{2}$$

$$\partial(\rho^* \mathbf{u}^*)/\partial t^* + \nabla^* \cdot (\rho^* \mathbf{u}^* \mathbf{u}^*) = -\nabla^* p^* - (\nabla^* \cdot \tau^*). \tag{3}$$

By using continuity to simplify Eq. (3) and viscous transfer for a Newtonian fluid, one can transform Eq. (3) into

$$\rho^*[\partial \mathbf{u}^*/\partial t^* + (\mathbf{u}^* \cdot \nabla^*)\mathbf{u}^*] = -\nabla^* p^* + \mu^*[4\nabla^*(\nabla^* \cdot \mathbf{u}^*)/3 - \nabla^* \times (\nabla^* \times \mathbf{u}^*)], \tag{4}$$

where μ^* is the dynamic viscosity.

To be general, dimensionless parameters are introduced. Spatial coordinates are hence normalized by a, while velocity and time are made dimensionless by a_0 and ω_0, respectively. In summary, we let

$$x = x^*/a, \quad r = r^*/a, \quad t = \omega_0 t^*, \quad \mathbf{u} = \mathbf{u}^*/a_0, \quad p = p^*/(\gamma p_0), \quad \text{and} \quad \rho = \rho^*/\rho_0, \tag{5}$$

where γ is the ratio of specific heats, and ρ_0 and p_0 are the stagnation density and pressure. Following this nomenclature, Eqs. (2) and (4) become

$$\omega \partial\rho/\partial t + \nabla \cdot (\rho \mathbf{u}) = 0, \tag{6}$$

$$\rho[\omega \partial \mathbf{u}/\partial t + (\mathbf{u} \cdot \nabla)\mathbf{u}] = -\nabla p + \mathrm{M}\varepsilon[4\nabla(\nabla \cdot \mathbf{u})/3 - \nabla \times (\nabla \times \mathbf{u})]. \tag{7}$$

Equations (6) and (7) employ the definitions of the nondimensional frequency $\omega \equiv \omega_0 a/a_0$, the suction Mach number $\mathrm{M} \equiv V_s/a_0$, and the small parameter $\varepsilon \equiv 1/\mathrm{Re}$.

B. Perturbed variables

With the introduction of small amplitude oscillations, the instantaneous pressure can be expressed as the linear sum of time-dependent and steady components:

$$p = p^{(0)} + \varepsilon_w p^{(1)} \exp(-it), \tag{8}$$

where $i = \sqrt{-1}$, $\varepsilon_w = A_p/(\gamma p_0)$, and $[p^{(0)}, p^{(1)}]$ are spatial functions. Unlike $p^{(1)}$, $p^{(0)}$ can be shown to be a constant at order $\mathcal{O}(\mathrm{M}^2)$, namely, $p^{(0)} = 1/\gamma + \mathcal{O}(\mathrm{M}^2)$. Noting that the mean flow solution is incompressible, small compressibility effects can only influence the time-dependent field. Density can thus be normalized by its mean component and expanded in a similar fashion viz.

$$\rho = 1 + \varepsilon_w \rho^{(1)} \exp(-it). \tag{9}$$

The total velocity can also be expanded as

$$\mathbf{u} = \mathrm{M}\mathbf{U} + \varepsilon_w \mathbf{u}^{(1)} \exp(-it), \tag{10}$$

where $\mathbf{U}$ represents the mean flow velocity normalized by V_s. Following Majdalani and Flandro,[34] we impose a constraint on the wave amplitude, namely,

$$\mathrm{M}^2 < \varepsilon_w < \mathrm{M}, \tag{11}$$

where $\mathrm{M} < 0.01$.

C. Leading-order decomposition

Equations (8)–(10) can be inserted back into Eqs. (6) and (7). The zeroth-order terms yield the mean flow equations

$$\nabla \cdot \mathbf{U} = 0, \tag{12}$$

$$\mathrm{M}^2(\mathbf{U} \cdot \nabla)\mathbf{U} = -\nabla p^{(0)} + \mathrm{M}^2\varepsilon[4\nabla(\nabla \cdot \mathbf{U})/3 - \nabla \times (\nabla \times \mathbf{U})]. \tag{13}$$

Following Berman,[5] a steady streamfunction can be defined by $\Psi = -xF(r)$. Subsequently, the velocity can be expressed by $(U_x, U_r) = [-xF'(r)/r, F(r)/r]$. By substituting these definitions into Eq. (13), Terrill has shown that $F = r^2$ provides the exact mean flow solution for the infinitely large suction case.[28] The mean pressure arising in this context can be integrated from Eq. (13) to obtain

$$p^{(0)}(x,r) = 1/\gamma - \mathrm{M}^2 r^2 (1 + x^2)/2. \tag{14}$$

D. Time-dependent equations

Terms of $\mathcal{O}(\varepsilon_w)$ in Eqs. (6) and (7) lead to

$$-i\omega\rho^{(1)} + \nabla \cdot \mathbf{u}^{(1)} = -\mathrm{M}\nabla \cdot (\rho^{(1)}\mathbf{U}), \tag{15}$$

$$-i\omega\mathbf{u}^{(1)} = -\mathrm{M}[\nabla(\mathbf{U} \cdot \mathbf{u}^{(1)}) - \mathbf{u}^{(1)} \times (\nabla \times \mathbf{U}) - \mathbf{U} \times (\nabla \times \mathbf{u}^{(1)})] - \nabla p^{(1)} + \mathrm{M}\varepsilon[4\nabla(\nabla \cdot \mathbf{u}^{(1)})/3 - \nabla \times (\nabla \times \mathbf{u}^{(1)})]. \tag{16}$$

Equations (15) and (16) describe the intimate coupling between mean and unsteady motions. They indicate that the wall suction velocity $\mathbf{U}$ can strongly influence the oscillatory flow motion.

IV. MOMENTUM TRANSPORT FORMULATION

A. Irrotational and solenoidal vectors

In order to proceed, temporal disturbances can be split into solenoidal and irrotational components.[35] Using a circumflex to denote the curl-free pressure-driven part, and a tilde for the divergence-free boundary-driven part, the time-dependent velocity component can be expressed as

$$\mathbf{u}^{(1)} = \hat{\mathbf{u}} + \tilde{\mathbf{u}}, \tag{17}$$

with

$$\nabla \times \mathbf{u}^{(1)} = \nabla \times \tilde{\mathbf{u}}, \quad p^{(1)} = \hat{p}, \quad \rho^{(1)} = \hat{\rho}. \tag{18}$$

This decomposition charges all vortices to the vortical field $\tilde{\mathbf{u}} = (\tilde{u}, \tilde{v})$, and compressibility sources and sinks to the acoustical field $\hat{\mathbf{u}} = (\hat{u}, \hat{v})$.

B. The linearized Navier-Stokes equations

Insertion of Eqs. (17) and (18) into Eqs. (15) and (16) leads to two independent sets that are coupled through the boundary conditions at the wall. These responses are byproducts of pressure-driven and vorticity-driven oscillation modes at $\mathcal{O}(\varepsilon_w)$. While the acoustical, compressible, and irrotational equations collapse into

$$-i\omega\hat{\rho} + \nabla \cdot \hat{\mathbf{u}} = -\mathrm{M}\nabla \cdot (\hat{\rho}\mathbf{U}), \tag{19}$$

$$-i\omega\hat{\mathbf{u}} = -\nabla\hat{p} + 4\mathrm{M}\varepsilon\nabla(\nabla\cdot\hat{\mathbf{u}})/3 - \mathrm{M}[\nabla(\hat{\mathbf{u}}\cdot\mathbf{U}) - \hat{\mathbf{u}}\times(\nabla\times\mathbf{U})], \tag{20}$$

the rotational and incompressible set comprises of

$$\nabla\cdot\tilde{\mathbf{u}} = 0, \tag{21}$$

$$-i\omega\tilde{\mathbf{u}} = -\mathrm{M}\varepsilon\nabla\times(\nabla\times\tilde{\mathbf{u}}) - \mathrm{M}[\nabla(\tilde{\mathbf{u}}\cdot\mathbf{U}) - \tilde{\mathbf{u}}\times(\nabla\times\mathbf{U}) - \mathbf{U}\times(\nabla\times\tilde{\mathbf{u}})]. \tag{22}$$

C. Coupling conditions

Two boundary conditions must be satisfied by the unsteady velocity component $\mathbf{u}^{(1)}$. These are the no-slip condition at the wall $u^{(1)}(x,1)=0$, and centerline symmetry, $\partial u^{(1)}(x,0)/\partial r = 0$.

D. Pressure-driven solution

When Eq. (19) is multiplied by $-i\omega$, the divergence of Eq. (20) can be evaluated; resulting terms can be added to produce the following wave equation:

$$\nabla^2\hat{p} + \omega^2\hat{p} = 4\mathrm{M}\varepsilon\nabla^2(\nabla\cdot\hat{\mathbf{u}})/3 - \mathrm{M}\{i\omega\nabla\cdot(\mathbf{U}\hat{p}) + \nabla^2(\hat{\mathbf{u}}\cdot\mathbf{U}) - \nabla\cdot[\hat{\mathbf{u}}\times(\nabla\times\mathbf{U})]\}. \tag{23}$$

At this juncture, a solution at $\mathcal{O}(\mathrm{M})$ can be achieved through separation of variables and closed-open boundary conditions. The ensuing acoustical pressure and velocity are

$$\hat{p} = \cos(\omega x) + \mathcal{O}(\mathrm{M}), \quad \hat{\mathbf{u}} = i\sin(\omega x)\mathbf{e}_x + \mathcal{O}(\mathrm{M}). \tag{24}$$

E. Vortical equations

Assuming that the ratio of the normal to axial velocity is of the same order as the Mach number [i.e. $\tilde{v}/\tilde{u} = \mathcal{O}(\mathrm{M})$], $\tilde{v}$ can be dropped at leading order. This assumption can be justified in view of the arguments presented by Flandro.[36] Applying this condition, along with the definition of the mean flow velocity, the axial momentum equation reduces to

$$i\mathrm{Sr}\tilde{u} = \frac{\partial(\tilde{u}\mathbf{U})}{\partial x} + v_0\frac{\partial\tilde{u}}{\partial r} - \frac{\varepsilon}{r}\frac{\partial}{\partial r}\left(r\frac{\partial\tilde{u}}{\partial r}\right) + \mathcal{O}(\mathrm{M}), \tag{25}$$

where $\mathrm{Sr} = \omega/\mathrm{M}$ is the Strouhal number. When expressed in terms of the mean flow streamfunction, Eq. (25) becomes

$$\left(i\mathrm{Sr} + \frac{F'}{r}\right)\tilde{u} = \frac{F}{r}\frac{\partial\tilde{u}}{\partial r} - \frac{xF'}{r}\frac{\partial\tilde{u}}{\partial x} - \frac{\varepsilon}{r}\frac{\partial}{\partial r}\left(r\frac{\partial\tilde{u}}{\partial r}\right) + \mathcal{O}(\mathrm{M}). \tag{26}$$

A solution for Eq. (26) will be presented next.

F. The separable boundary-layer equation

A solution for Eq. (26) can be developed through the use of separation of variables. Assuming the form

$$\tilde{u}(x,r) = X(x)Y(r), \tag{27}$$

substitution into Eq. (26) leads to

$$\frac{x}{X}\frac{\mathrm{d}X}{\mathrm{d}x} = \frac{F}{F'Y}\frac{\mathrm{d}Y}{\mathrm{d}r} - \frac{\varepsilon r}{F'Y}\frac{\mathrm{d}^2Y}{\mathrm{d}r^2} - \frac{\varepsilon}{F'Y}\frac{\mathrm{d}Y}{\mathrm{d}r} - \frac{ir\mathrm{Sr}}{F'} - 1 = \kappa_n, \tag{28}$$

where $\kappa_n > 0$ is the separation eigenvalue. Integration of the x equation can be performed easily and then inserted into Eq. (27). The outcome is

$$\tilde{u}(x,r) = \sum_n c_n x^{\kappa_n} Y_n(r), \tag{29}$$

where c_n is the integration constant for each κ_n. Satisfaction of the no-slip condition at the wall requires setting the acoustical and vortical velocity components equal and opposite at $r=1$. One finds

$$\tilde{u}(x,1) = -i\sin(\omega x). \tag{30}$$

Using a series expansion of the sine function, and setting the result equal to Eq. (29), one gets

$$\sum_n c_n x^{\kappa_n} Y_n(1) = -i\sum_{n=0}^{\infty}\frac{(-1)^n(\omega x)^{2n+1}}{(2n+1)!}. \tag{31}$$

Equating terms necessitates that

$$\kappa_n = 2n+1, \quad c_n = -i\frac{(-1)^n\omega^{2n+1}}{(2n+1)!}, \quad Y_n(1) = 1, \tag{32}$$

where $n = 0,1,2,\ldots,\infty$. The rotational velocity component becomes

$$\tilde{u}(x,r) = -i\sum_{n=0}^{\infty}\frac{(-1)^n(\omega x)^{2n+1}}{(2n+1)!}Y_n(r). \tag{33}$$

In order to bring closure to Eq. (33), Y_n needs to be determined from Eq. (28). One finds that Y_n must be obtained from the doubly perturbed boundary-value problem, namely,

$$\varepsilon\frac{\mathrm{d}^2Y_n}{\mathrm{d}r^2} + [(\varepsilon - F)/r]\frac{\mathrm{d}Y_n}{\mathrm{d}r} + [i\mathrm{Sr} + (2n+2)F'/r]Y_n = 0, \tag{34}$$

where

$$Y_n(1) = 1, \quad Y_n'(0) = 0. \tag{35}$$

These two boundary conditions stem from the no-slip and core symmetry requirements.

V. BOUNDARY-LAYER ANALYSIS

Substitution of Terrill's mean flow solution $F = r^2$ into Eq. (34) leads to

$$\varepsilon\frac{\mathrm{d}^2Y_n}{\mathrm{d}r^2} + (-r + \varepsilon/r)\frac{\mathrm{d}Y_n}{\mathrm{d}r} + (i\mathrm{Sr} + 4n + 4)Y_n = 0. \tag{36}$$

In what follows, Eq. (36) will be solved using the method of matched-asymptotic expansions. To that end, the perturbation parameters need to be first identified. Since our concern is with solutions corresponding to large Re, the primary perturbation parameter is clearly $\varepsilon = \mathrm{Re}^{-1} \ll 1$. Furthermore, one must recognize that the condition of $\mathrm{Sr} \gg 1$ is necessary to ensure a sufficiently oscillatory flow. It may be instructive to note that, according to (25), the Strouhal number depends on the product of the circular frequency and tube radius ($\omega_0 a$) divided by the suction velocity V_s. Since V_s is usually two to three orders of magnitude smaller than the speed of sound, Sr is about two to three orders of magnitude

larger than the aeroacoustic Strouhal number based on a_0 instead of V_s. Recalling that the latter extends over $[10^{-3},10]$ with a peak in the noise spectrum at $\mathrm{Sr}\approx 0.2$, the current Strouhal number extends over the range $[1,10^3]$ with typically reported values of $\mathrm{Sr}\approx 20-50$.

Asymptotic approximations to Eq. (36) depend on the development of a relationship between the two perturbation parameters present in the problem. By inspection of numerical simulations carried out for the large suction case, one comes to the conclusion that the problem exhibits a typical second-order wave-type response that bears a strong resemblance to a critically damped wave. On that account, a distinguished limit will be needed to relate ε and Sr in a manner to produce the expected response.

To start, an order of magnitude relationship between the control parameters must be posited. Without loss in generality, one can let

$$\mathrm{Sr}\sim\mathcal{O}(\varepsilon^{-\zeta}). \tag{37}$$

Subsequently, rescaling of the viscous domain requires a distortion of the independent variable in the form

$$1-r=\varepsilon^k z. \tag{38}$$

In order to determine the distinguished limit, one may apply the stretching transformation and use $\mathrm{Sr}=\varepsilon^{-\zeta}$ in Eq. (36). The result is

$$\varepsilon^{1-2k}\frac{\mathrm{d}^2Y_n}{\mathrm{d}z^2}+\varepsilon^{-k}(r-\varepsilon/r)\frac{\mathrm{d}Y_n}{\mathrm{d}z}+[i\varepsilon^{-\zeta}+(4n+4)]Y_n=0. \tag{39}$$

For a critically damped response to occur near the wall, a balance between all three terms in Eq. (39) must be established. Clearly, all terms will be in balance when $\zeta=k=1$. These distinctive orders indicate that the boundary-layer thickness is of $\mathcal{O}(\varepsilon)$ and that

$$\mathrm{Sr}=\mathcal{O}(\varepsilon^{-1}). \tag{40}$$

It may be interesting to note that these distinguished limits are dissimilar from those realized in the injection flow analog,[37–42] including those arising in the rectangular cavity.[1,2] The disparity can be attributed to the reversal in the physics of the problem, namely, in the relocation of the viscous boundary layer to the vicinity of the suction wall.

VI. MATCHED-ASYMPTOTIC EXPANSIONS

A. The relevant scales

In order to proceed, one has to identify the length scale needed to magnify the thin viscous region near the wall. From the foregoing order of magnitude analysis, the relevant scales can be recognized to be $r=r$ in the outer domain and

$$z=(1-r)/\varepsilon \tag{41}$$

in the inner region. Solving the problem with matched-asymptotic expansions involves the formulation of two separate solutions over the domain of interest. While Eq. (36) is only valid in the outer domain (i.e., the inviscid region), a transformed equation is needed to capture the rapid variations near the wall (inside the viscous boundary layer). In both cases, we find it convenient to multiply Eq. (36) by r and write the governing equation as

$$\varepsilon r\frac{\mathrm{d}^2Y_n}{\mathrm{d}r^2}+(-r^2+\varepsilon)\frac{\mathrm{d}Y_n}{\mathrm{d}r}+r[i\mathrm{Sr}+(4n+4)]Y_n=0. \tag{42}$$

B. The outer solution

Using regular perturbations to construct the outer solution Y_n^o, one may start by putting

$$Y_n^o=Y_0^o+\varepsilon Y_1^o+\mathcal{O}(\varepsilon^2). \tag{43}$$

Inserting Eq. (43) into Eq. (42) gives

$$\varepsilon r\frac{\mathrm{d}^2Y_0^o}{\mathrm{d}r^2}-r^2\frac{\mathrm{d}Y_0^o}{\mathrm{d}r}-r^2\varepsilon\frac{\mathrm{d}Y_1^o}{\mathrm{d}r}+\varepsilon\frac{\mathrm{d}Y_0^o}{\mathrm{d}r}+r[(4n+4)+i\mathrm{Sr}]\times(Y_0^o+\varepsilon Y_1^o)+\mathcal{O}(\varepsilon^2)=0. \tag{44}$$

Keeping in mind that $\mathrm{Sr}=\mathcal{O}(\varepsilon^{-1})$, the equations defining the first two terms in the outer solution become

$$i\mathrm{Sr}Y_0^o=0, \tag{45}$$

$$i\mathrm{Sr}\varepsilon Y_1^o=r^2\frac{\mathrm{d}Y_0^o}{\mathrm{d}r}-r(4n+4)Y_0^o. \tag{46}$$

Solving these equations leads to

$$Y_0^o=Y_1^o=0,\quad Y_n^o=0+\mathcal{O}(\varepsilon^2). \tag{47}$$

C. The inner solution

Having realized that the outer solution is zero, the stretching transformation must now be applied to the original coordinate in order to obtain the inner equation. This procedure converts Eq. (42) into

$$(1-\varepsilon z)\frac{\mathrm{d}^2Y_n^i}{\mathrm{d}z^2}+[1-\varepsilon(2z+1)+\varepsilon^2z]\frac{\mathrm{d}Y_n^i}{\mathrm{d}z}+(\varepsilon-\varepsilon^2z)\times[(4n+4)+i\mathrm{Sr}]Y_n^i=0. \tag{48}$$

The inner solution can be similarly expanded using $Y_n^i=Y_0^i+\varepsilon Y_1^i+\mathcal{O}(\varepsilon^2)$. The outcome is

$$(1-\varepsilon z)\frac{\mathrm{d}^2Y_0^i}{\mathrm{d}z^2}+(\varepsilon-\varepsilon^2z)\frac{\mathrm{d}^2Y_1^i}{\mathrm{d}z^2}+[1-\varepsilon(2z+1)+\varepsilon^2z]\times\left(\frac{\mathrm{d}Y_0^i}{\mathrm{d}z}+\varepsilon\frac{\mathrm{d}Y_1^i}{\mathrm{d}z}\right)+(\varepsilon-\varepsilon^2z)[(4n+4)+i\mathrm{Sr}]\times(Y_0^i+\varepsilon Y_1^i)=0. \tag{49}$$

Since the inner equation is of second order, two conditions must be imposed on the inner solution at each perturbation level. While the first can be determined from the no-slip at the wall, the second must be deduced by matching with the outer domain. Using Eq. (35) and the expansion for Y_n^i, the boundary condition at the wall gives

$$Y_0^i(z=0)=1,\quad Y_1^i(z=0)=0. \tag{50}$$

At this juncture, the leading and first-order correction terms can be readily found. From Eq. (49), the $\mathcal{O}(1)$ equation reads

$$\frac{d^2Y_0^i}{dz^2}+\frac{dY_0^i}{dz}+i\mathrm{Sr}\varepsilon Y_0^i=0, \tag{51}$$

wherefore

$$Y_0^i=c_1\exp[\tfrac{1}{2}(\sqrt{1-4i\mathrm{Sr}\varepsilon}-1)z] + c_2\exp[-\tfrac{1}{2}(\sqrt{1-4i\mathrm{Sr}\varepsilon}+1)z]. \tag{52}$$

Straightforward application of the boundary condition at the wall yields

$$c_2=1-c_1, \tag{53}$$

so that

$$Y_0^i=c_1\exp[\tfrac{1}{2}(\sqrt{1-4i\mathrm{Sr}\varepsilon}-1)z] + (1-c_1)\exp[-\tfrac{1}{2}(\sqrt{1-4i\mathrm{Sr}\varepsilon}+1)z]. \tag{54}$$

Next, the $\mathcal{O}(\varepsilon)$ equation can be collected from Eq. (49). One obtains

$$\frac{d^2Y_1^i}{dz^2}+\frac{dY_1^i}{dz}+i\mathrm{Sr}\varepsilon Y_1^i=z\frac{d^2Y_0^i}{dz^2}+(2z+1)\frac{dY_0^i}{dz} -(4n+4-i\mathrm{Sr}\varepsilon z)Y_0^i. \tag{55}$$

While the homogeneous solution can be evaluated by inspection via

$$Y_{1,\mathrm{h}}^i=B_1\exp[\tfrac{1}{2}(\sqrt{1-4i\mathrm{Sr}\varepsilon}-1)z] + B_2\exp[-\tfrac{1}{2}(\sqrt{1-4i\mathrm{Sr}\varepsilon}+1)z], \tag{56}$$

the right-hand side of Eq. (55) can be rearranged into

$$c_1[\tfrac{1}{4}(\sqrt{1-4i\mathrm{Sr}\varepsilon}-1)^2z+(z+\tfrac{1}{2})(\sqrt{1-4i\mathrm{Sr}\varepsilon}-1) -(4n+4-i\mathrm{Sr}\varepsilon z)]\exp[\tfrac{1}{2}(\sqrt{1-4i\mathrm{Sr}\varepsilon}-1)z] +(1-c_1)[\tfrac{1}{4}(\sqrt{1-4i\mathrm{Sr}\varepsilon}+1)^2z-(z+\tfrac{1}{2})(\sqrt{1-4i\mathrm{Sr}\varepsilon} +1)-(4n+4-i\mathrm{Sr}\varepsilon z)\exp[-\tfrac{1}{2}(\sqrt{1-4i\mathrm{Sr}\varepsilon}+1)z]. \tag{57}$$

A particular solution must therefore be assumed such that

$$Y_{1,\mathrm{p}}^i=(B_3z+B_4z^2)\exp[\tfrac{1}{2}(\sqrt{1-4i\mathrm{Sr}\varepsilon}-1)z] + (B_5z+B_6z^2)\exp[-\tfrac{1}{2}(\sqrt{1-4i\mathrm{Sr}\varepsilon}+1)z]. \tag{58}$$

After differentiating and substituting Eq. (58) into the left-hand side of Eq. (55), equating terms of order 1 and z^2 requires that

$$B_3=c_1\left[\frac{1}{2}-\frac{(4n+\frac{9}{2})}{\sqrt{1-4i\mathrm{Sr}\varepsilon}}\right],\quad B_4=0,$$

$$B_5=(1-c_1)\left[\frac{1}{2}+\frac{(4n+\frac{9}{2})}{\sqrt{1-4i\mathrm{Sr}\varepsilon}}\right],\quad B_6=0. \tag{59}$$

By writing $Y_1^i=Y_{1,\mathrm{h}}^i+Y_{1,\mathrm{p}}^i$ and enforcing Eq. (50), the inner solution turns into

$$Y_n^i=\left\{c_1-B_2\varepsilon+c_1z\varepsilon\left[\frac{1}{2}-\frac{(4n+\frac{9}{2})}{\sqrt{1-4i\mathrm{Sr}\varepsilon}}\right]\right\} \times\exp[\tfrac{1}{2}(\sqrt{1-4i\mathrm{Sr}\varepsilon}-1)z] +\left\{(1-c_1)+B_2\varepsilon+(1-c_1)z\varepsilon\left[\frac{1}{2}+\frac{(4n+\frac{9}{2})}{\sqrt{1-4i\mathrm{Sr}\varepsilon}}\right]\right\} \times\exp[-\tfrac{1}{2}(\sqrt{1-4i\mathrm{Sr}\varepsilon}+1)z]. \tag{60}$$

D. Asymptotic matching

Inner and outer solutions can be readily matched using Prandtl's matching principle.[43] By requiring the inner solution in the outer domain to match the outer solution in the inner domain, one may set

$$Y_n^i(z\to\infty)=Y_n^o(r\to0)=Y_{n,\mathrm{cp}}, \tag{61}$$

where $Y_{n,\mathrm{cp}}$ represents the common part in the overlap region shared by both inner and outer solutions. In our problem, both the outer and common parts are zero. The inner solution in the outer domain will also vanish according to Eq. (61) if, and only if, $c_1=B_2=0$. These constants bring closure to the inner solution by permitting the construction of a uniformly valid composite solution. Hence, by adding the inner and outer solutions, less $Y_{n,\mathrm{cp}}$, one finally obtains

$$Y_n(r)=\{1+(1-r)[\tfrac{1}{2}+(4n+\tfrac{9}{2})/\sqrt{1-4i\mathrm{Sr}\varepsilon}]\} \times\exp[-\tfrac{1}{2}(\sqrt{1-4i\mathrm{Sr}\varepsilon}+1)(1-r)/\varepsilon]. \tag{62}$$

E. The oscillatory velocity

Insertion of Eq. (62) into Eq. (33) results in an expression for the rotational velocity component. The addition of the acoustical component, given by Eq. (24), enables us to express the total axial velocity as an infinite sum, namely,

$$u^{(1)}(x,r)=i\left(\sin(\omega x)-\sum_{n=0}^{\infty}\frac{(-1)^n(\omega x)^{2n+1}}{(2n+1)!} \times\left\{1+(1-r)\left[\frac{1}{2}+\frac{(4n+\frac{9}{2})}{\sqrt{1-4i\mathrm{Sr}\varepsilon}}\right]\right\} \times\exp[-\tfrac{1}{2}(\sqrt{1-4i\mathrm{Sr}\varepsilon}+1)(1-r)/\varepsilon]\right). \tag{63}$$

Since $(1-r)$ is small near the wall, one may use $n=0$ in the secondary term arising from the first-order inner correction. The resulting expression can be summed, at leading order, over all eigenvalues, and placed in closed form by recognizing and grouping the implicit sine function expansion. This manipulation produces

$$u^{(1)}(x,r)=i\sin(\omega x)\{1-[1+\tfrac{1}{2}(1-r)(1+9/\sqrt{1-4i\mathrm{Sr}\varepsilon})] \times\exp[-\tfrac{1}{2}(\sqrt{1-4i\mathrm{Sr}\varepsilon}+1)(1-r)/\varepsilon]\}. \tag{64}$$

Being practically equivalent to Eq. (63), this formula completes our derivation of the acoustico-vortical contribution. Equation (64) clearly displays the key parameters affecting the unsteady wave behavior.

The foregoing methodology sketches the procedural steps needed to arrive at a field approximation based on a matched-asymptotic solution of the vorticity wave. The same approach can be employed in other suction-driven problems exhibiting more sophisticated mean flow functions. For appreciable suction, however, an exact solution of the rotational contribution is possible. This will be presented next.

VII. EXACT SOLUTION

A. Motivation

For the case of $F=r^2$, Eq. (34) can be solved exactly. This requires setting

$$X=\phi, \quad B(X)=\psi Y_n, \tag{65}$$

where ϕ and ψ are functions of the radial coordinate r. These transformations yield

$$\frac{\mathrm{d}Y_n}{\mathrm{d}r}=-\frac{\psi'}{\psi^2}B+\frac{\phi'}{\psi}\frac{\mathrm{d}B}{\mathrm{d}X}, \quad \frac{\mathrm{d}^2Y_n}{\mathrm{d}r^2}=\frac{\phi'^2}{\psi}\frac{\mathrm{d}^2B}{\mathrm{d}X^2} + \left(\frac{\phi''}{\psi}-\frac{2\phi'\psi'}{\psi^2}\right)\frac{\mathrm{d}B}{\mathrm{d}X}-\left(\frac{\psi''}{\psi^2}-\frac{2\psi'^2}{\psi^3}\right)B, \tag{66}$$

where primes stand for differentiation with respect to r. Substitution into Eq. (34) gives

$$\frac{\mathrm{d}^2B}{\mathrm{d}X^2}+\frac{1}{\phi'^2}\left(\phi''-\frac{2\phi'\psi'}{\psi}-r\,\mathrm{Re}\,\phi'+\frac{\phi'}{r}\right)\frac{\mathrm{d}B}{\mathrm{d}X}+\left[-\frac{\psi''}{\psi} + \frac{2\psi'^2}{\psi^2}+\frac{r\,\mathrm{Re}\,\psi'}{\psi}-\frac{\psi'}{r\psi}+\mathrm{Re}(i\mathrm{Sr}+4n+4)\right]\frac{B}{\phi'^2}=0. \tag{67}$$

At this point, ψ and ϕ are chosen so that the variable coefficients in Eq. (67) are turned into pure constants. For that purpose, the coefficient of the first derivative is suppressed via

$$\phi''-2\phi'\psi'/\psi-r\,\mathrm{Re}\,\phi'+\phi'/r=0,$$

$$\psi'/\psi=\tfrac{1}{2}(\phi''/\phi'-r\,\mathrm{Re}+r^{-1}). \tag{68}$$

Integrating Eq. (68) gives $\psi=T_0\sqrt{r\phi'}\exp(-\mathrm{Re}\,r^2/4)$, where T_0 is constant. Equation (67) simplifies into

$$B_{XX}+[\mathrm{Re}(i\mathrm{Sr}+4n+4)\phi'^{-2}+\beta]B=0, \tag{69}$$

where

$$\beta=\frac{1}{\phi'^2}\left[-\frac{\psi''}{\psi}+\frac{2\psi'^2}{\psi^2}+\left(r\,\mathrm{Re}-\frac{1}{r}\right)\frac{\psi'}{\psi}\right]. \tag{70}$$

By setting $\mathrm{Re}(i\mathrm{Sr}+4n+4)/\phi'^2=\mathrm{const}$, one obtains $\phi'=\sqrt{\mathrm{Re}}$ and $X=\phi=r\sqrt{\mathrm{Re}}$. Without losing generality, one puts $T_0=1/\sqrt[4]{\mathrm{Re}}$ so that $\psi(r)=\sqrt{r}\exp(-\mathrm{Re}\,r^2/4)$. The outcome is

$$B_{XX}+[\sigma-\tfrac{1}{4}(X^2-1/X^2)]B=0; \quad \sigma=5+4n+iS \tag{71}$$

B. Complete solution

At this point, two additional variable transformations are needed. The first applies to the dependent variable via $H(X)=B(X)\sqrt{X}$. Equation (71) becomes

$$H_{XX}-H_X/X+(\sigma-\tfrac{1}{4}X^2+1/X^2)H=0. \tag{72}$$

The second transformation, namely, $Z=X^2/2$, affects the independent variable. This results in

$$\frac{\mathrm{d}^2H}{\mathrm{d}Z^2}+\left(-\frac{1}{4}+\frac{\sigma}{2Z}+\frac{1}{4Z^2}\right)H=0, \tag{73}$$

whose solution can be written as

$$H(Z)=C_1M_{(1/2)\,\sigma,0}(Z)+C_2W_{(1/2)\,\sigma,0}(Z), \tag{74}$$

where C_1 and C_2 are constants to be determined from boundary conditions; the functions M and W, on the other hand, are the Whittaker functions of the first and second kind. The Whittaker functions are related to the Kummer or confluent hypergeometric functions through[44]

$$M_{\kappa,\mu}(Z)=Z^{(1/2)+\mu}e^{-(1/2)Z}\Phi(\tfrac{1}{2}+\mu-\kappa,1+2\mu;Z),$$

$$W_{\kappa,\mu}(Z)=Z^{(1/2)+\mu}e^{-(1/2)Z}\Psi(\tfrac{1}{2}+\mu-\kappa,1+2\mu;Z), \tag{75}$$

wherefrom

$$H(Z)=\sqrt{Z}\exp(-\tfrac{1}{2}Z)[C_1\Phi(\tfrac{1}{2}-\tfrac{1}{2}\sigma,1;Z) + C_2\Psi(\tfrac{1}{2}-\tfrac{1}{2}\sigma,1;Z)]. \tag{76}$$

Returning to original variables, one gets

$$Y_n(r)=\sqrt[4]{\mathrm{Re}/4}[C_1\Phi(\tfrac{1}{2}-\tfrac{1}{2}\sigma,1;\tfrac{1}{2}\mathrm{Re}\,r^2) + C_2\Psi(\tfrac{1}{2}-\tfrac{1}{2}\sigma,1;\tfrac{1}{2}\mathrm{Re}\,r^2)]. \tag{77}$$

Note that $\sqrt[4]{\mathrm{Re}/4}$ is a constant that can be absorbed into C_1 and C_2. Thus, without loss in generality, one puts

$$Y_n(r)=C_1\Phi(\tfrac{1}{2}-\tfrac{1}{2}\sigma,1;\tfrac{1}{2}\mathrm{Re}\,r^2) + C_2\Psi(\tfrac{1}{2}-\tfrac{1}{2}\sigma,1;\tfrac{1}{2}\mathrm{Re}\,r^2),$$

$$Y_n'(r)=r\,\mathrm{Re}(\tfrac{1}{2}-\tfrac{1}{2}\sigma)[C_1\Phi(\tfrac{3}{2}-\tfrac{1}{2}\sigma,2;\tfrac{1}{2}\mathrm{Re}\,r^2) - C_2\Psi(\tfrac{3}{2}-\tfrac{1}{2}\sigma,2;\tfrac{1}{2}\mathrm{Re}\,r^2)]. \tag{78}$$

To find C_2, $\Psi(a,b;z)$ must be expressed in terms of $\Phi(a,b;z)$ using[44]

$$\Psi(a,b;x)=\frac{\pi}{\sin(\pi b)}\left[\frac{\Phi(a,b;x)}{\Gamma(1+a-b)\Gamma(b)}-x^{1-b}\frac{\Phi(1+a-b,2-b;x)}{\Gamma(a)\Gamma(2-b)}\right]. \quad (79)$$

This expression leads to an infinite value at the core for $b>1$ except when $C_2=0$. The remaining C_1 is determined using the boundary condition at the wall. One finds

$$Y_n(r)=\Phi(\tfrac{1}{2}-\tfrac{1}{2}\sigma,1;\tfrac{1}{2}\mathrm{Re}\,r^2)/\Phi(\tfrac{1}{2}-\tfrac{1}{2}\sigma,1;\tfrac{1}{2}\mathrm{Re}), \quad (80)$$

which indicates that the characteristic coordinate scales with $r\sqrt{\mathrm{Re}/2}$. Following the same lines as before, one can sum the acoustical and vortical contributions to obtain the unsteady velocity component. This takes the form

$$u^{(1)}(x,r)=i\left[\sin(\omega x)-\sum_{n=0}^{\infty}\frac{(-1)^n(\omega x)^{2n+1}\Phi(-2n-2-\frac{1}{2}i\mathrm{Sr},1;\frac{1}{2}\mathrm{Re}\,r^2)}{(2n+1)!\Phi(-2n-2-\frac{1}{2}i\mathrm{Sr},1;\frac{1}{2}\mathrm{Re})}\right]. \quad (81)$$

Unlike the matched-asymptotic solution given by Eq. (62), the physical clarity of the exact solution is encumbered by the infinite summation of the Kummer function.

VIII. DISCUSSION

A. A formerly tested methodology

The decomposition of the time-dependent governing equations presented in Sec. IV, during the momentum transport formulation, was first introduced by Flandro[42] and further developed by Majdalani and Roh.[38] For injection-driven flows with superimposed oscillations, a similar analytical framework has provided accurate flow field predictions. Those could be substantiated using fully nonlinear computational models. The asymptotic approximations obtained previously were also shown to agree favorably with experimental data obtained in cold-flow simulations of transpiring surfaces.[39–42] Although the physical nature of the problem changes when suction is introduced, the assumptions used in reducing the governing equations remain valid, regardless of the inflow or outflow boundary conditions. By analogy with the injection-driven problem, one can expect a comparable level of agreement between the asymptotic formulations given here and either numerical or experimental studies of the model at hand. However, in the absence of experimental measurements to compare with, numerical simulations must be resorted to.

B. Numerical confirmation

Due to the lack of experimental data for the suction-driven flow, we have compared the matched-asymptotic expansion to a numerical solution of Eq. (36) obtained from a code that was originally developed for injection-driven flows by Majdalani and Van Moorhem.[39] The same code was tested by comparing its results to the exact solution derived in Sec. VII. The algorithm employs a fixed step fifth-order Runge-Kutta method with shooting to handle the boundary conditions. For the suction case, the step size used was 10^{-6} on a normalized interval. In former studies,[39–41] the same code was shown to provide satisfactory agreement with experimental data. Therein, the code was also shown to closely match computational data obtained independently by Yang and Roh who utilized a fully compressible, finite-volume Navier-Stokes solver.[45]

C. Graphical confirmation

Figure 2 illustrates the agreement between the exact or numerical solutions and Eq. (62). Over typical ranges of physical parameters, the graphical comparison clearly indicates that the matched-asymptotic solution is in close agreement with the numerical results. Graphically, the accuracy of the approximate formulation is seen to increase with increasing Reynolds and Strouhal numbers. This observation is reassuring since it indicates that the solution exhibits the proper asymptotic behavior as $\varepsilon=\mathrm{Re}^{-1}\to 0$ and $\mathrm{Sr}^{-1}\to 0$. It is also satisfying to note the nearly critical damped-wave response. This rapid damping in both depth and amplitude is consistent with the arguments introduced in Sec. V regarding the scaling orders of Sr and ε. Also note that the wave behavior is different from the highly under-damped wave solution associated with injection-driven flows. In the latter, numerous peaks of diminishing amplitude appear as the distance from the wall is increased.[1]

In order to assess the truncation error associated with Eq. (62), the maximum absolute error between asymptotics and numerics is shown in Fig. 3 for the first three eigenvalues and a range of Sr and Re. When plotted versus ε, this error is seen to exhibit a clear asymptotic order as $\varepsilon\to 0$. It also decreases in magnitude with successive increases in Sr. It can also be seen that the slope of the error curves and, in turn, the order of the truncation error approach unity for

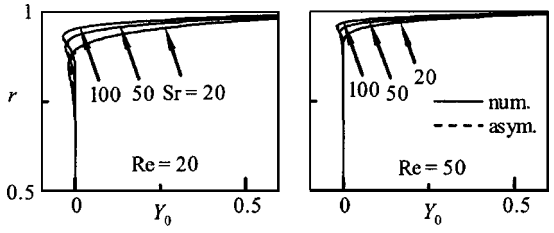

FIG. 2. Here Y_n is plotted for $n=0$ over a range of Reynolds and Strouhal numbers. The figures show the slightly under-damped response at Re=20 and 50.

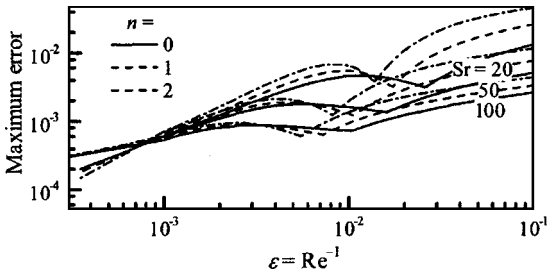

FIG. 3. Plot of the maximum error in the approximate solution versus ε.

sufficiently small ε. This confirms the order claimed for this approximation. In particular, it may be useful to note that the slight increase in the error intercept at higher eigenvalues does not affect the summed up solution. This is due to the rapid convergence of the series in Eq. (63) as n is increased.

D. Variation of flow parameters

The four subsets of Fig. 4 illustrate the effect of varying either the suction velocity or the oscillation frequency on the time-dependent solution. In all four cases, the velocity is seen to be a wave traveling in time. While a viscous and rotational layer is present near the wall, a broad inviscid and irrotational region covers the remaining domain. Interestingly, the unsteady velocity reaches a maximum value inside the viscous layer where a small velocity overshoot is realized near the wall. This phenomenon is well known as Richardson's annular effect and seems to be characteristic of oscillatory flows in tubes and channels with and without wall permeation.[46] The small percentage overshoot that accompanies a suction-driven flow is of the same order as that associated with the exact Sexl profile inside a nonporous tube. It is significantly smaller than the 100% overshoot (i.e., velocity doubling) that recurs near the walls of injection-driven flows.

According to the theory of laminar periodic flows, one could expect the magnitude of the velocity overshoot to increase at higher oscillation frequencies.[46] The reason is this. As the Strouhal number is increased, the spatial wavelength diminishes, being inversely proportional to Sr. The first oscillation peak stemming from a favorable coupling between acoustical and vortical waves will then form closer to the wall. Since the rotational component diminishes with the distance from the wall, a larger vortical contribution augments the acoustical wave when their coupling occurs closer to the wall (e.g., at higher frequencies). The reduction in spatial wavelength at higher Strouhal numbers increases the rate of viscous dissipation and causes the boundary-layer thickness to decrease.[47] The latter is often referred to as the penetration depth and is a measure of the viscous and rotational layer above the solid boundary.

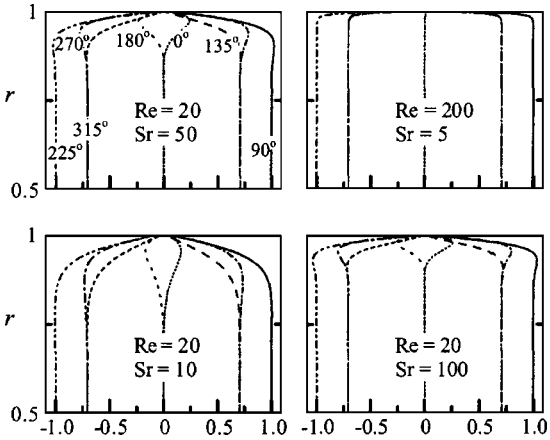

FIG. 4. The oscillatory velocity $u^{(1)}\exp(-it)$ is shown at four different times for $m=1$ and $x/l=0.5$. Angles in the figures represent dimensionless time. Properties correspond to an order of magnitude variation in Reynolds and Strouhal numbers.

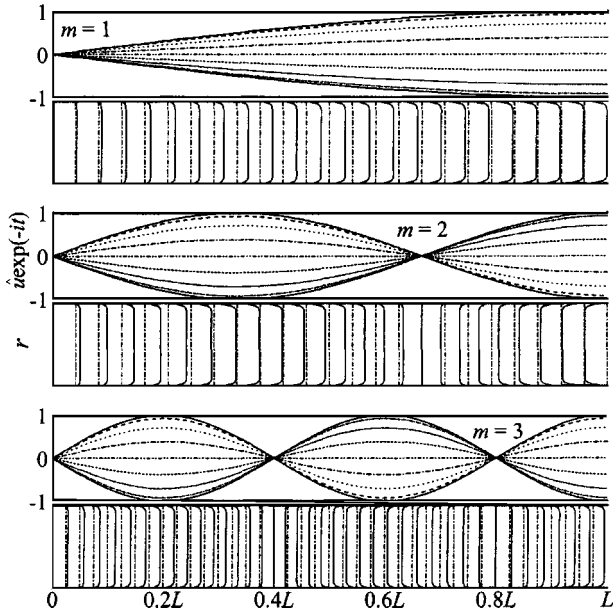

FIG. 5. The spatial distribution of the oscillatory velocity $u^{(1)}\exp(-it)$ is illustrated for the first three acoustical oscillation modes by plotting the velocity modulus at several evenly spaced axial positions for Re=20 and Sr=10. The corresponding longitudinal mode shapes of the acoustical velocity component are also shown at nine equally dispersed times. In addition to the head end location, the smallest disturbances occur at the nth internal acoustical node located at $x^*/L=n/(m-\frac{1}{2})$, $n<m$, $m=1,2,3$, etc.

The top two subsets in Fig. 4 illustrate the effects of increasing the Reynolds number while decreasing the Strouhal number via an order of magnitude increase in V_s. As the suction speed is increased, the rotational layer is reduced in both depth and overshoot. While the reduction in overshoot can be attributed to the smaller vortical contribution associated with a smaller Sr, the smaller depth may be attributed to the increased Re. Evidently, the increased fluid withdrawal rate has the effect of attracting the viscous layer closer to the wall.

The bottom two subsets, on the other hand, confirm the previous statements made regarding the oscillation frequency. Clearly, through an order of magnitude increase in Sr, the penetration depth is decreased, while Richardson's effect is made more appreciable.

E. Oscillation modes

In closing, we use Fig. 5 to show the spatial evolution of the oscillatory velocity for the first three oscillation modes. Also plotted are the amplitudes of the inviscid velocity at nine equally scattered times. This is done to illustrate the

strong correspondence between the pressure-driven inviscid mode shapes and the spatial distribution of the total velocity. Since the rotational contribution always decays away from the walls, it is clear that the inviscid solution dominates near the core. The spatial amplitude of the oscillatory velocity is hence controlled by the pressure-driven mode shapes associated with the inviscid wave. Except for the small viscous layer that is drawn to the wall by hard suction, the flow is primarily irrotational. In addition to the head end location where no oscillations can be entertained, the weakest disturbances take place in the vicinity of nth internal acoustical nodes. This is due to the smallest wave amplitudes being located at $x/l=n/(m-\frac{1}{2})$ for all $n<m$ as shown on the graph.

In this article, the main thrust has been placed on presenting the procedural steps needed to obtain an unsteady flow approximation based on matched-asymptotic expansions of the vortical wave contribution. For the special case of appreciable wall suction, an exact solution was also possible. Despite its algebraic opacity, the exact solution served a dual purpose by helping to validate both numerics and asymptotics. In later work, we hope to extend this analysis to an oscillating gas with arbitrary levels of suction.

ACKNOWLEDGMENT

The authors are deeply grateful for the support received from the National Science Foundation under Grant No. CMS-0353518.

[1] J. Majdalani, "Vortical and acoustical mode coupling inside a two-dimensional cavity with transpiring walls," J. Acoust. Soc. Am. **106**, 46–56 (1999).
[2] J. Majdalani, "Improved solution for the vortical and acoustical mode coupling inside a two-dimensional cavity with porous walls," J. Acoust. Soc. Am. **109**, 475–479 (2001).
[3] R. G. Gutman, *Membrane Filtration* (Adam Hilger, Bristol, UK, 1987).
[4] V. Nassehi, "Modelling of combined Navier-Stokes and Darcy flows in crossflow membrane filtration," Chem. Eng. Sci. **53**(6), 1253–1265 (1998).
[5] A. S. Berman, "Laminar flow in channels with porous walls," J. Appl. Phys. **24**(9), 1232–1235 (1953).
[6] A. S. Berman, "Effects of porous boundaries on the flow of fluids in systems with various geometries," Proceedings of the Second United Nations International Conference on the Peaceful Uses of Atomic Energy (1958), Vol. 4, pp. 351–358.
[7] A. S. Berman, "Laminar flow in an annulus with porous walls," J. Appl. Phys. **29**(1), 71–75 (1958).
[8] J. M. Drazen, R. D. Kamm, and A. S. Slutsky, "High frequency ventilation," Physiol. Rev. **64**(2), 505–543 (1984).
[9] C. Y. Wang, "Pulsatile flow in a porous channel," Trans. AMSE: Ser. E J. Appl. Mech. **38**, 553–555 (1971).
[10] Y. C. Fung and C. S. Yih, "Peristaltic transport," J. Appl. Mech. **35**, 669–675 (1968).
[11] H. N. Chang, J. S. Ha, J. K. Park, I. H. Kim, and H. D. Shin, "Velocity field of pulsatile flow in a porous tube," J. Biomech. **22**(11-12), 1257–1262 (1989).
[12] G. D. Raithby and D. C. Knudsen, "Hydrodynamic development in a duct with suction and blowing," Trans. ASME: Ser. E **41**, 896–902 (1974).
[13] J. P. Hartnell and E. R. G. Eckert, "Mass-transfer cooling in a laminar boundary layer with constant fluid properties," Trans. ASME **79**, 247–254 (1957).
[14] G. Avalon, G. Casalis, and J. Griffond, "Flow instabilities and acoustic resonance of channels with wall injection," presented at the AIAA 98-3218, Cleveland, OH, 1998.
[15] G. Casalis, G. Avalon, and J.-P. Pineau, "Spatial instability of planar channel flow with fluid injection through porous walls," Phys. Fluids **10**(10), 2558–2568 (1998).
[16] J. Griffond, G. Casalis, and J.-P. Pineau, "Spatial instability of flow in a semiinfinite cylinder with fluid injection through its porous walls," Eur. J. Mech. B/Fluids **19**(1), 69–87 (2000).
[17] M. B. Zaturska, P. G. Drazin, and W. H. H. Banks, "On the flow of a viscous fluid driven along a channel by suction at porous walls," Fluid Dyn. Res. **4**(3), 151–178 (1988).
[18] C. L. Taylor, W. H. H. Banks, M. B. Zaturska, and P. G. Drazin, "Three-dimensional flow in a porous channel," Q. J. Mech. Appl. Math. **44**(1), 105–133 (1991).
[19] W. H. H. Banks and M. B. Zaturska, "On flow through a porous annular pipe," Phys. Fluids **4**(6), 1131–1141 (1992).
[20] M. B. Zaturska and W. H. H. Banks, "Suction-driven flow in a porous pipe," J. Appl. Math. Mech. **75**(1), 21–30 (1995).
[21] W. A. Robinson, "The existence of multiple solutions for the laminar flow in a uniformly porous channel with suction at both walls," J. Eng. Math. **10**(1), 23–40 (1976).
[22] K.-G. Shih, "On the existence of solutions of an equation arising in the theory of laminar flow in a uniformly porous channel with injection," SIAM J. Appl. Math. **47**(3), 526–533 (1987).
[23] S. P. Hastings, C. Lu, and A. D. MacGillivray, "A boundary value problem with multiple solutions from the theory of laminar flow," SIAM J. Math. Anal. **23**(1), 201–208 (1992).
[24] C. Lu, "On the existence of multiple solutions of a boundary value problem arising from laminar flow through a porous pipe," Cana. Appl. Mathematics Q. **2**(3), 361–393 (1994).
[25] S. W. Yuan and A. B. Finkelstein, "Laminar pipe flow with injection and suction through a porous wall," Trans. ASME: Ser. E **78**(3), 719–724 (1956).
[26] S. W. Yuan, "Further investigation of laminar flow in channels with porous walls," J. Appl. Phys. **27**(3), 267–269 (1956).
[27] J. R. Sellars, "Laminar flow in channels with porous walls at high suction Reynolds numbers," J. Appl. Phys. **26**(4), 489–490 (1955).
[28] R. M. Terrill and P. W. Thomas, "On laminar flow through a uniformly porous pipe," Appl. Sci. Res. **21**, 37–67 (1969).
[29] R. M. Terrill, "Laminar flow through a porous tube," J. Fluids Eng. **105**, 303–307 (1983).
[30] R. M. Terrill, "On some exponentially small terms arising in flow through a porous pipe," Q. J. Mech. Appl. Math. **26**(3), 347–354 (1973).
[31] J. Majdalani, "Vorticity dynamics in isobarically closed porous channels. Part I: standard perturbations," J. Propul. Power **17**(2), 355–362 (2001).
[32] J. Majdalani and T. S. Roh, "Vorticity dynamics in isobarically closed porous channels. Part II: space-reductive perturbations," J. Propul. Power **17**(2), 363–370 (2001).
[33] R. B. Bird, W. E. Stewart, and E. N. Lightfoot, *Transport Phenomena* (J. Wiley, New York, 1960).
[34] J. Majdalani and G. A. Flandro, "The oscillatory pipe flow with arbitrary wall injection," Proc. R. Soc. **458**(2022), 1621–1651 (2002).
[35] R. H. Cantrell and R. W. Hart, "Interaction between sound and flow in acoustic cavities: mass, momentum, and energy considerations," J. Acoust. Soc. Am. **36**, 697–706 (1964).
[36] G. A. Flandro, "Effects of vorticity on rocket combustion stability," J. Propul. Power **11**(4), 607–625 (1995).
[37] J. Majdalani, "The oscillatory channel flow with arbitrary wall injection," J. Appl. Math. Phys. **52**(1), 33–61 (2001).
[38] J. Majdalani and T. S. Roh, "The oscillatory channel flow with large wall injection," Proc. R. Soc. **456**(1999), 1625–1657 (2000).
[39] J. Majdalani and W. K. Van Moorhem, "Improved time-dependent flowfield solution for solid rocket motors," AIAA J. **36**(2), 241–248 (1998).
[40] J. Majdalani, G. A. Flandro, and T. S. Roh, "Convergence of two flowfield models predicting a destabilizing agent in rocket combustion," J. Propul. Power **16**(3), 492–497 (2000).
[41] J. Majdalani and W. K. Van Moorhem, "Laminar cold-flow model for the internal gas dynamics of a slab rocket motor," J. Aerosp. Sci. Technol. **5**(3), 193–207 (2001).
[42] G. A. Flandro, "Effects of vorticity transport on axial acoustic waves in a solid propellant rocket chamber," in *Combustion Instabilities Driven by Thermo-Chemical Acoustic Sources* (American Society of Mechanical Engineers, New York, 1989), Vol. NCA 4, HTD 128, pp. 53–61.
[43] C. M. Bender and S. A. Orszag, *Advanced Mathematical Methods for Scientists and Engineers* (McGraw-Hill, New York, 1978).
[44] M. Abramowitz and I. A. Stegun, *Handbook of Mathematical Functions* (National Bureau of Standards, New York, 1964).

[45] T. S. Roh, I. S. Tseng, and V. Yang, ''Effects of acoustic oscillations on flame dynamics of homogeneous propellants in rocket motors,'' J. Propul. Power **11**(4), 640–650 (1995).
[46] N. Rott, ''Theory of time-dependent laminar flows,'' in *High Speed Aerodynamics and Jet Propulsion–Theory of Laminar Flows*, edited by F. K. Moore (Princeton U.P., Princeton, NJ, 1964), Vol. IV, pp. 395–438.
[47] H. Schlichting, *Boundary-Layer Theory*, 7th ed. (McGraw-Hill, New York, 1979).